NOAA Technical Report ERL 375-WPL 48

Feasibility of Atmospheric Temperature Sensing from Ocean Data Buoys by Microwave Radiometry

E. R. Westwater
M. T. Decker
F. O. Guiraud

July 1976

U.S. DEPARTMENT OF COMMERCE
National Oceanic and Atmospheric Administration
Environmental Research Laboratories

NOAA Technical Report ERL 375-WPL 48

Feasibility of Atmospheric Temperature Sensing from Ocean Data Buoys by Microwave Radiometry

E. R. Westwater
M. T. Decker
F. O. Guiraud

Wave Propagation Laboratory
Boulder, Colorado

July 1976

U.S. DEPARTMENT OF COMMERCE
Elliot Richardson, Secretary

National Oceanic and Atmospheric Administration
Robert M. White, Administrator

Environmental Research Laboratories
Wilmot Hess, Director

CONTENTS

FEASIBILITY OF ATMOSPHERIC TEMPERATURE SENSING FROM OCEAN DATA BUOYS BY MICROWAVE RADIOMETRY

E. R. Westwater, M. T. Decker and F. O. Guiraud

The feasibility of measuring atmospheric temperature structure by using a microwave radiometer mounted on an ocean-based data buoy has been investigated with simulated measurements. The accuracy of layer-averaged temperature retrievals was studied as a function of radiometer noise level, various choices of frequency, number of channels, layer pressure thickness, clear vs. cloudy skies, and five ocean climatologies. A three-frequency zenith measurement of O_2 thermal emission (instrumental noise of 0.5 K) made during clear conditions can be mathematically inverted to infer 100-mb layer averages of temperature with rms accuracies that range from 0.5 K at the lowest altitudes to 1.7 K at 500 mb. To correct for cloud emission, additional brightness measurements are required near 21 and 31 GHz. With the five-channel system the rms temperature retrieval error for cloudy conditions is degraded (relative to clear air) by at most 0.3 K. The two cloud-correcting channels also yield measurements of integrated liquid water and water vapor content.

1. INTRODUCTION

Ocean-based data buoys are currently providing useful surface meteorological observations of temperature, pressure, humidity and wind. The meteorological utility of buoy observations would be much enhanced if vertical profiles of these meteorological parameters could be measured. In response to a request for technical assistance from the NOAA Data Buoy Office (NDBO), we are reporting on the scientific feasibility of instrumenting an ocean buoy with a microwave radiometric temperature sensor with the purpose of inferring information about temperature structure from passive measurements of thermal radiation emitted from the atmosphere. (Complementary aspects of this investigation, such as engineering feasibility and cost analysis have been undertaken by other agencies.)

Previous field experiments (Hosler and Lemmons, 1972; Miner et al., 1972; Snider, 1972; Westwater et al., 1975) have demonstrated that, under clear conditions, ground-based microwave radiometry can recover smoothed features of vertical temperature profiles. For some applications, such as numerical forecasting, fine structure is not of primary interest, and accurate determination of layer-averaged temperature would be quite useful. Accuracy requirements for a buoy-mounted upper air sounding system have been developed by the National Weather Service (Hallgren, 1974):

> "The system should provide: ... the average temperature for each 100-mb layer up to a specified level, with an accuracy of ± 1°C. We would like to have data for layers up to 500 mb or higher if technically feasible. For some purposes, including some of the models, data up through the 850-mb layer would be useful and worth acquiring. Humidity data would add further to the value of the sounding; however, this is not stated as a requirement because of anticipated difficulties in the development of sensors."

Furthermore, a system must operate under a wide variety of cloud conditions and consequently, a substantial portion of our effort is devoted to the problem of retrieving temperature profiles and layer averages from cloud-contaminated brightness temperature observations.

Our paper is arranged as follows: Section 2 briefly reviews the theory of microwave absorption and emission in clear air and clouds. This is followed in section 3 by a derivation of the statistical inversion equations used to infer layer averages from microwave thermal noise observations. Our retrieval method appropriate to cloudy conditions is a sequence of two distinct algorithms. First, "equivalent clear-air brightness temperatures" are inferred from multi-spectral cloud-contaminated brightness observations. Then we invert the equivalent observations to derive temperature information. In section 4, we discuss step one of the retrieval process by introducing our method for deriving equivalent clear-air observations. After a discussion of our data base and cloud models, we complete the section by presenting calculations to demonstrate the accuracy of step one. In section 5, we apply the second stage of our profile inversion algorithms to determine the accuracy to which layer-averaged temperature can be inferred from brightness temperature observations under both clear and cloudy conditions. Simulations to estimate buoy motion effects on microwave brightness temperature are given in an appendix. We conclude with recommendations for further work to verify the favorable conclusions of the theoretical study.

2. MICROWAVE ATTENUATION AND EMISSION IN CLEAR AND CLOUDY ATMOSPHERES

Quantitative radiometric remote sensing of atmospheric temperature and humidity structure requires a mathematical relationship between measurements of radiant power and desired parameters. This relationship usually requires the solution of two problems in radiative transfer: (i) the direct problem; i.e., given the state of the atmosphere (temperature and composition profiles, etc), what is the radiant power?, and (ii) the indirect problem; i.e., given a set of radiation measurements, what is the state of the atmosphere? The solution of (ii) almost always requires the solution of (i). In this section we briefly review the formal solution to the direct problem, namely the radiative transfer equation, and discuss the calculations required by this equation.

2.1 Radiative Transfer Equation

Measurements of microwave radiant power are commonly expressed as an equivalent black body temperature, or brightness temperature, T_b. Except during rain, atmospheric scattering is small relative to absorption. For a non-scattering atmosphere in local thermodynamic equilibrium, the downward brightness temperature at frequency ν is given by

$$T_b(\nu) = T_b^{(ext)} \tau_\nu + \int_0^\infty T \alpha_\nu \exp \left(\int_0^s \alpha_\nu(s')ds' \right) ds, \qquad (1)$$

where

T = absolute temperature (K),

α_ν = absorption coefficient (km^{-1})

$T_b^{(ext)}$ = brightness temperature external to the earth's atmosphere (K),

τ_ν = transmission through the atmosphere,

and

s = path length from the receiver to emitting volume (km).

In the troposphere, microwave absorption is due principally to molecular resonances of O_2 (60 GHz) and H_2O (22 GHz) and to clouds and rain. In general, the absorption is a strong function of composition and a weak function of temperature. Thus, around 22 GHz, the emission varies principally because of variations in water concentration, whereas at 60 GHz, the emission from the well-mixed constituent O_2 depends mainly on temperature.

2.2 Clear Attenuation

Beginning with the classic theoretical papers by Van Vleck (1947a, 1947b) on microwave absorption by molecular O_2 and H_2O, a large amount of theoretical, laboratory, and atmospheric research has been devoted to the understanding of attenuation in the clear air. As a consequence, the knowledge of molecular absorption parameters and of molecular pressure broadening theory has steadily increased. Two recent advances are of note. The first is the development of the dispersion spectroscopy technique by Liebe and its application to the determination of the spectroscopic parameters of H_2O (Liebe, 1969) and O_2 (Liebe, 1975). The second is Rosenkranz's (1975) theoretical attenuation model which accounts for overlapping lines in the oxygen complex. Liebe's measurements of oxygen dispersion over a wide range of frequencies and pressures will soon be completed. These

measurements, when interpreted by Rosenkranz's theory, should allow accurate calculations of brightness throughout the oxygen band.

Calculations of O_2 and H_2O attenuation are included in Figure 1. Because Liebe's measurements are not yet completed, we have used the (reasonably adequate) O_2 linewidth parameters determined by Carter et al., (1968). From 50 to 70 GHz these calculations are accurate to about 8%. Details of our clear air calculations are given by Snider and Westwater (1969).

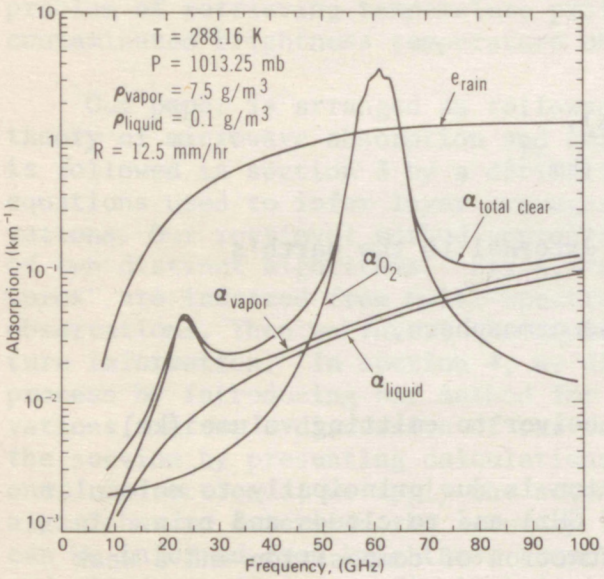

Figure 1. Microwave atmospheric absorption due to clear air, clouds, and rain.
α = absorption coefficient.
e = attenuation coefficient.

2.3 Attenuation by Clouds and Rain

Attenuation from a distribution of spherical particles of known dielectric properties can be calculated by classical electromagnetic theory. Depending on the ratio of particle size to wavelength, simplicity or complexity prevails. In the domain where this ratio is small, called the Rayleigh region, attenuation is independent of size distribution and is directly proportional to total mass of droplets. In addition, scattering is negligible relative to absorption. For large particles, Mie theory must be used, and attenuation depends on size distribution in both absorption and scattering. For our purposes, we will consider water clouds with modal radii less than 50 μm to be in the Rayleigh region for frequencies less than 100 GHz. Calculations of water absorption for a cloud liquid water content of $\rho_{liquid} = 0.1$ g/m^3 are shown in Figure 1. Depending on the frequency, spherical ice particles absorb from 1 to 2 orders of magnitude less than an equivalent amount of water.

In contrast to non-precipitating clouds, rain (and hail) both scatters and absorbs microwave energy. The attenuation coefficient e must be calculated from Mie theory for both absorption and scattering coefficients.

Calculations of e for a moderate rain of 12.5 mm/hr are also shown in Figure 1. We assumed a Laws and Parsons (1943) size distribution for this rainrate (liquid water content = 0.6 g/m^3). It is clear that rain dominates all other sources of attenuation except in the vicinity of the oxygen complex.

2.4 Cloud Emission

The atmospheric thermal emission spectrum in the presence of a cloud can differ considerably from that obtained under clear conditions. In detail, the amount of contrast depends on the height profiles of temperature, humidity, and liquid content. However, the largest contribution to the difference is the liquid thickness with the emission being relatively insensitive to the height and geometric thickness of the cloud (see section 4).

A calculation of the emission from a moderately dense cloud is shown in Figure 2. It is immediately clear that, even in the oxygen complex, cloud effects can be large. Our technique for correcting for clouds will be discussed in section 4.

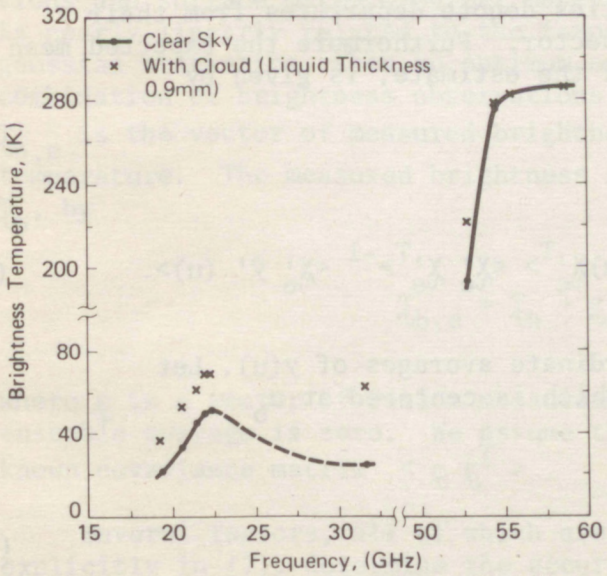

Figure 2. Microwave thermal emission from clear and cloudy sky.

3. STATISTICAL RETRIEVAL OF LAYER AVERAGED TEMPERATURE PROFILES UNDER CLEAR CONDITIONS

Statistical retrieval algorithms have been extensively used to extract temperature profiles from both microwave (Waters et al., 1975; Westwater et al., 1975) and infrared (Smith et al., 1970; Rodgers, 1970) radiation measurements. In addition, these algorithms are quite useful in predicting a priori expected retrieval accuracies if realistic estimates of measurement uncertainties are available. In this section, we briefly review the linear statistical retrieval algorithm, and we detail its modification for retrieving linear averages. Finally, we give a typical example of its application.

Abstractly, deriving a profile from a set of radiance observations, is an example of a general statistical problem of estimating a quantity $y(u)$ that is related in a known way to a vector of imperfect measurements $\underset{\sim}{X}_e = \{X_{e,i},\ i = 1,2,\ldots M\}$. Here, the continuous variable u may be taken to be any profile coordinate, restricted to a finite range $a \leq u \leq b$, such as pressure P, $\ln P$, or height. The minimum variance estimate $\hat{y}(u)$ of the departure of $y(u)$ from its known ensemble average $\langle y(u)\rangle$ is given by Deutsch (1965)

$$\hat{y}'(u) = \langle y'(u)\, \underset{\sim}{X}_e'^{T}\rangle \langle \underset{\sim}{X}_e'\, \underset{\sim}{X}_e'^{T}\rangle^{-1}\, \underset{\sim}{X}_e' \,. \tag{2}$$

Our notation is: A^T is the matrix transpose of A, S^{-1} is the matrix inverse of the square matrix S, primed quantities denote departures from their ensemble averages, and $\underset{\sim}{X}$ is a column vector. Furthermore the expected mean square error, or residual, $R(\hat{y}(u))$, of the estimate, is given by

$$R(\hat{y}(u)) \equiv \langle (y(u) - \hat{y}(u))^2 \rangle$$

$$= \langle (y'(u))^2 \rangle - \langle y'(u) \underset{\sim}{X}_e'^{T}\rangle \langle \underset{\sim}{X}_e'\, \underset{\sim}{X}_e'^{T}\rangle^{-1} \langle \underset{\sim}{X}_e'\, \hat{y}'(u)\rangle. \tag{3}$$

Consider estimates of linear coordinate averages of $y(u)$. Let $\bar{y}(u_o)$ denote the linear average of y which is centered at u_o

$$\bar{y}(u_o) \equiv \frac{1}{\Delta} \int_{u_o - \frac{\Delta}{2}}^{u_o + \frac{\Delta}{2}} y(u)\, du, \tag{4}$$

where the thickness, Δ, is such that $a \leq u_o - \frac{\Delta}{2} \leq u_o + \frac{\Delta}{2} \leq b$. Since the linear coordinate averages and ensemble averages commute, i.e.,

$$\langle \bar{y}(u_o) \rangle = \overline{\langle y(u_o) \rangle} \ , \tag{5}$$

it follows from (2) that

$$\overline{\hat{y}(u_o)} = \hat{\bar{y}}(u_o) = \frac{1}{\Delta} \int_{u_o - \frac{\Delta}{2}}^{u_o + \frac{\Delta}{2}} \langle y'(u) \underset{\sim}{X}_e'^{T} \rangle \langle \underset{\sim}{X}_e' \underset{\sim}{X}_e'^{T} \rangle^{-1} \underset{\sim}{X}_e' \, du. \tag{6}$$

Substituting (4), (5), and (6) into (3) yields

$$R(\overline{\hat{y}(u_o)}) \equiv \langle (\overline{y(u_o)} - \overline{\hat{y}(u_o)})^2 \rangle = \frac{1}{\Delta^2} \int_{u_o - \frac{\Delta}{2}}^{u_o + \frac{\Delta}{2}} du_1 \int_{u_o - \frac{\Delta}{2}}^{u_o + \frac{\Delta}{2}} du_2$$

$$\{ \langle y'(u_1) \, y'(u_2) \rangle - \langle y'(u_1) \underset{\sim}{X}_e'^{T} \rangle \langle \underset{\sim}{X}_e' \underset{\sim}{X}_e'^{T} \rangle^{-1} \langle \underset{\sim}{X}_e' \, y'(u_2) \rangle \} \ . \tag{7}$$

Equations (6) and (7) form the basis of our subsequent analysis for determining the accuracy to which layer averages may be inferred.

The data vector $\underset{\sim}{X}_e$ can be formed from various combinations of observations and surface meteorological observations. Since the microwave brightness is nearly linearly related to the temperature profile, and if we assume gaussian statistics, then an optimum estimator can be formed from a linear combination of brightness observations, i.e., $\underset{\sim}{X}_e = [\underset{\sim}{T}_{b,e}, T_o]$, where $\underset{\sim}{T}_{b,e}$ is the vector of measured brightness and T_o is the known surface temperature. The measured brightness is related to the "true brightness", $\underset{\sim}{T}_b$, by

$$\underset{\sim}{T}_{b,e} = \underset{\sim}{T}_b + \underset{\sim}{\varepsilon} \ , \tag{8}$$

where $\underset{\sim}{\varepsilon}$ is a vector of random measurement (and other) errors whose ensemble average is zero. We assume these errors are described by a known covariance matrix $\langle \underset{\sim}{\varepsilon} \underset{\sim}{\varepsilon}^{T} \rangle$.

Several factors, all of which are contained either implicitly or explicitly in (7), determine the accuracy of temperature T(u) retrieval during clear conditions. Among them are

(a) weighting functions -- their number, shape, and degree of independence,

(b) the noise level of the instrument $\langle \underset{\sim}{\varepsilon} \underset{\sim}{\varepsilon}^{T} \rangle$,

(c) climatology -- this enters through the covariance function $\langle T'(u_1)T(u_2)\rangle$ and includes statistical variability and the correlation of the profile between different pressure levels, and

(d) the pressure thickness Δ of the retrieved layer.

An example of accuracy prediction for a particular climatology is shown in Figure 3. Here we assume three vertical brightness measurements of rms accuracy 0.5 K at 54.0, 55.4, and 58.8 GHz. We used a priori statistics (918 profiles) gathered for two years of data 1967-1968 for weather ship E(Lat. 35:00 N, Long. 48:00 W). Curve 1 shows the a priori profile variation about the known surface temperature and curve 2 is the rms accuracy of the profile retrieval. The rms accuracies in retrievals of 100 mb and 200 mb layer averages are shown by curves 3 and 4. For this pressure range and thickness, the difference in rms accuracy between averaging with respect to ℓn P and with respect to P was less than 0.01 K. Several features of these curves are of note. First, all retrievals exhibit a large reduction in variance, even at high altitudes. Second, the improvement in accuracy of the layer averages over point retrievals is substantial below about 750 mb. Finally, at high altitudes, there is little difference in accuracy between point and lyaer-average retrievals. This is because of the poor spatial resolution of the point retrievals at these altitudes.

A large number of curves like those in Figure 3 were analyzed as a part of the data buoy radiometer feasibility study. Before presenting the summary of the results, we must first discuss our method of cloud correction, and the degree to which clouds degrade the temperature retrievals.

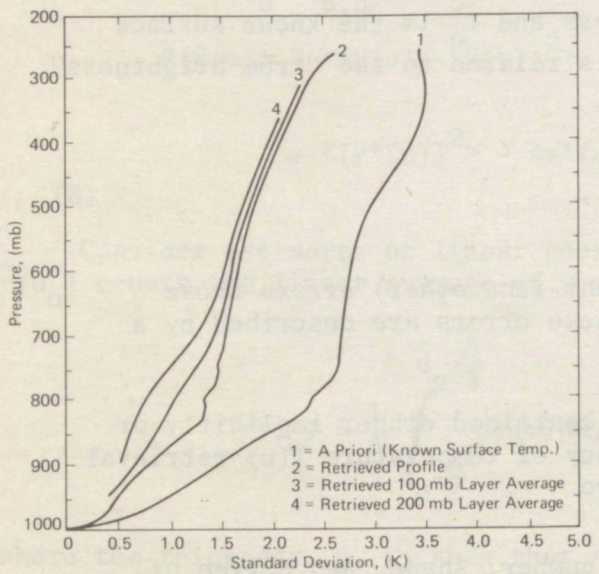

Figure 3. Rms errors in temperature retrieval for Weather Ship E during clear conditions. Radiometer noise level = 0.5 K. Frequency = 54.0, 55.4, and 58.8 GHz.

4. ESTIMATION OF CLEAR AIR BRIGHTNESS FROM CLOUDY EMISSION DATA

4.1 Inversion Algorithm

Thermal emission in the oxygen complex depends on the temperature profile, and to a degree, on water vapor and cloud moisture. As shown in section 2, cloud emission can introduce non-negligible departures from the corresponding emission from clear air. However, since microwave emission below about 45 GHz is insensitive to temperature structure and depends strongly on water, it is plausible that measurements in the oxygen complex could be supplemented with water sensitive measurements to correct for clouds. Since the lower frequency emission depends both on water vapor and liquid water, two frequencies are required to separate the water phases. Our technique then is to estimate the equivalent clear air brightness temperature $\hat{T}_b^{(eqv)}(O_2)$, from the corresponding cloudy measurement, $T_b^{(cld)}(O_2)$, and two supplementary measurements. Similar work has been published recently by Fowler et al. (1975). Let us call the measurement most sensitive to clouds $T_b(\text{cloud})$ and the measurement most sensitive to vapor $T_b(\text{vapor})$. In a procedure identical to our profile retrieval algorithm, we use a data vector comprising $T_b^{(cld)}(O_2)$, $T_b(\text{cloud})$, and $T_b(\text{vapor})$ (and perhaps, higher order products of these quantities) as a minimum variance estimator of $T_b^{(eqv)}(O_2)$ in (2). Our statistical ensemble is representative of both clouds and receiver noise. For thermal profile retrieval, the clear air equivalent T_b measurements are then used in the previous statistical retrieval algorithm, but with a different effective noise level. As we illustrate in section 4.3, the numerical value of this noise level depends, to a certain extent, on the range of liquid water thickness present in the cloud ensemble.

In using the algorithm presented above we assume that it is known whether or not clouds are present. Several techniques might be considered to provide this information. Optical color photography gives good information in high contrast situations but would tend to be unreliable for stratiform clouds, unusable at night, and difficult to implement for remote operation. It may be possible to use the two microwave measurements, $T_b(\text{cloud})$ and $T_b(\text{vapor})$, to categorize sky conditions as clear or cloudy, or even into sub-categories that depend on the amount of liquid water present. The degree to which this kind of categorization can be made and the resulting implications for effective noise levels of the equivalent clear air brightness temperature are being investigated. Additional information could be obtained from an infrared precision radiation thermometer (Platt, 1973). In addition to information on cloud presence (or absence) this instrument would provide information on cloud temperatures that would be useful in correcting for cloud emission. Finally, it might be feasible to apply a single algorithm to all cases, both clear and cloudy, without significant degradation in resulting effective noise levels.

4.2 Cloud Models

In section 4.1, we presented an algorithm for estimating clear brightness temperature from a set of cloudy measurements. Calculations to assess the accuracy to which this may be achieved require representative ensembles of cloud conditions (realistic statistical distributions of base height, thickness, liquid water content, droplet size distribution, etc.). Our ensembles were constructed as follows: We obtained two years of radiosonde soundings from each of five weather ships. These sets were searched for "clouds". A radiosonde profile was assumed to contain a cloud if at any point the relative humidity (RH) exceeded 95%. Base heights were taken to be the (interpolated) levels at which the RH first exceeded 95% and the thicknesses were determined using the points at which the humidity dropped below 95%. With this RH criterion for cloud existence, about 25% of the 6337 profiles contained clouds and about 10% of these contained two or more layers. Details of the cloud data base are shown in Table 1.

To keep the number of cloud emission calculations within reasonable bounds, not all of these profiles were used. From each of the five stations, about 50 cloud profiles were chosen randomly. Since liquid density is not measured by radiosondes, completion of our ensemble required modeling of this parameter. Assuming that the liquid density within a given cloud was constant with height, the modeling was done as follows: From the geometric thickness of each of these clouds, three values of liquid density were determined using the cloud thickness- liquid density models of Figure 4. These models attempt to cover a reasonable range of observed liquid densities for non-precipitating clouds, and restrict thin clouds to have low densities. In all, we generated a total of 720 cloudy profiles.

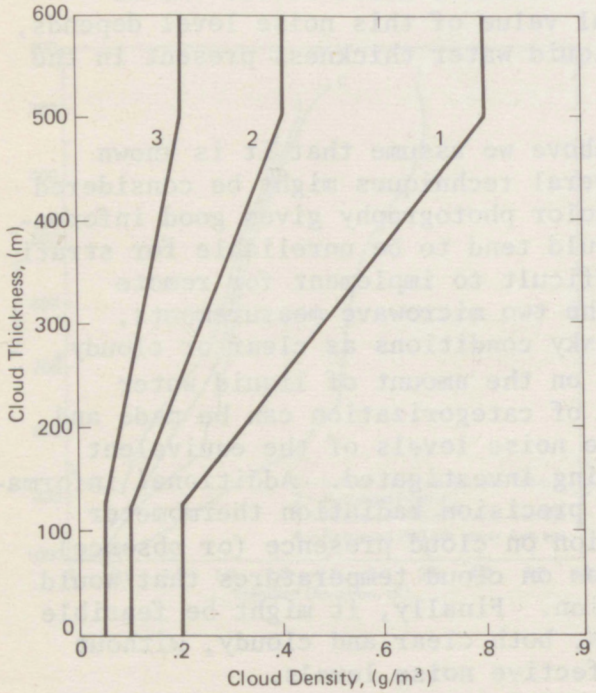

Figure 4. Cloud thickness — liquid density model used in thermal emission simulations.

TABLE 1.

Description of Radiosonde Profiles
Used in This Study

STATION	LAT.	LONG.	TIME PERIOD	NO. OF PROFILES	NO. WITH "CLOUDS"
P	50:00 N	145:00 W	1966-1967	1485	343
D	44:00 N	41:00 W	1967-1968	1329	467
H	36:40 N	69:35 W	1952/07-1954/06	1302	69
E	35:00 N	48:00 W	1967-1968	918	223
N	30:00 N	140:00 W	1967-1968	1303	373

NOTE: A radiosonde profile was assumed to contain a cloud if at any point the relative humidity equaled or exceeded 95%.

To investigate the statistical characteristics of these clouds, we performed histogram analyses on each data set and on the composite of all five sets. The histograms for cloud base temperature (C), cloud base height (km), cloud thickness (km), and liquid water thickness (mm) are shown in Figures 5-8. These figures show that the ensembles contain a wide range of variation of the four cloud parameters and hence, can provide a stringent test of our hypothesis that we can correct for clouds without knowledge of the details of cloud structure.

4.3 Numerical Results

We are trying to estimate the accuracy to which clear air brightness temperature can be inferred from a set of cloud-contaminated emission measurements. For a given angle of observation, it is clear that this accuracy will depend on frequency, on the noise level of the channels, and on the range of climatological variables encountered. Because of buoy motion, we restrict ourselves to the zenith direction only (see Appendix). Our analysis is as follows: For each profile in the ensemble, clear and cloudy zenith brightness temperatures were calculated at several frequencies in the oxygen complex and also at 19.35, 20.6, 21.5, 22.0, 22.235, and 31.65 GHz. Of these latter choices, 20.6 GHz and 31.65 GHz were the most promising and other frequencies were not considered further. For each weather ship, about 150 calculations were made for each frequency. For these frequencies, Table 2 shows the rms differences between calculated clear and cloudy T_b's (no measurement errors). These rms differences are consistent with our single case study of section 2.4 and demonstrate that cloud correction is necessary

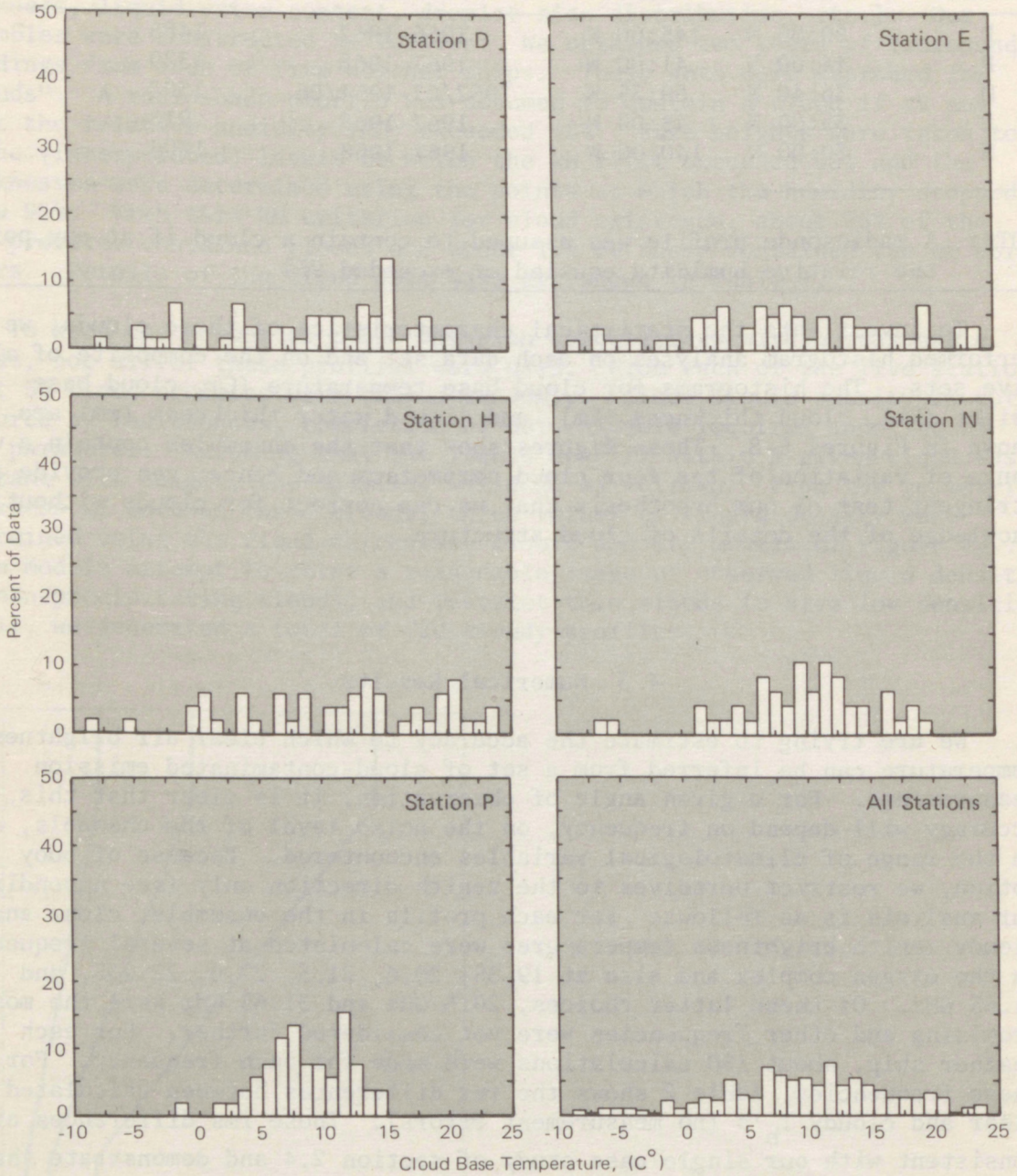

Figure 5. Histograms of cloud base temperature.

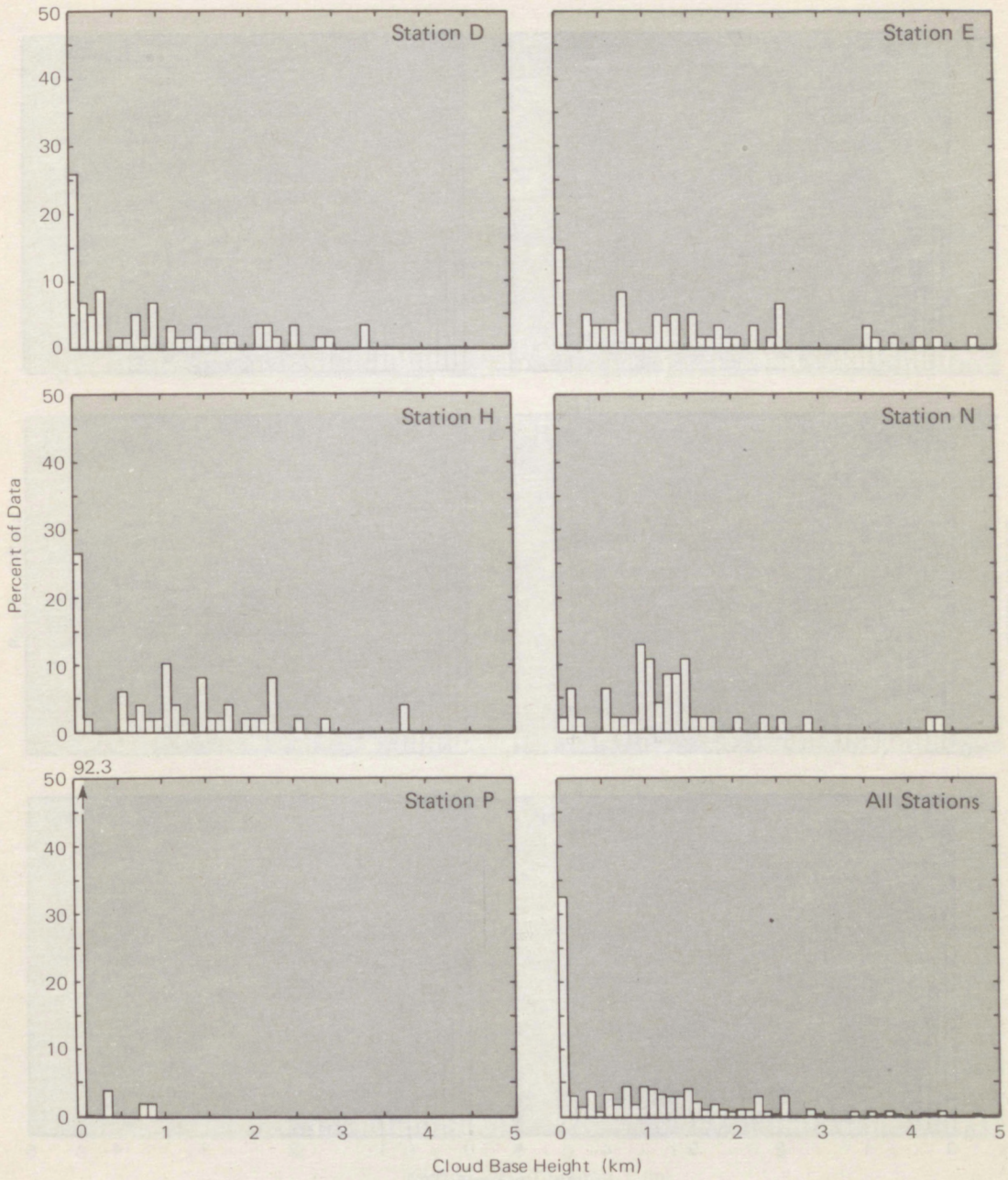

Figure 6. Histograms of cloud base height.

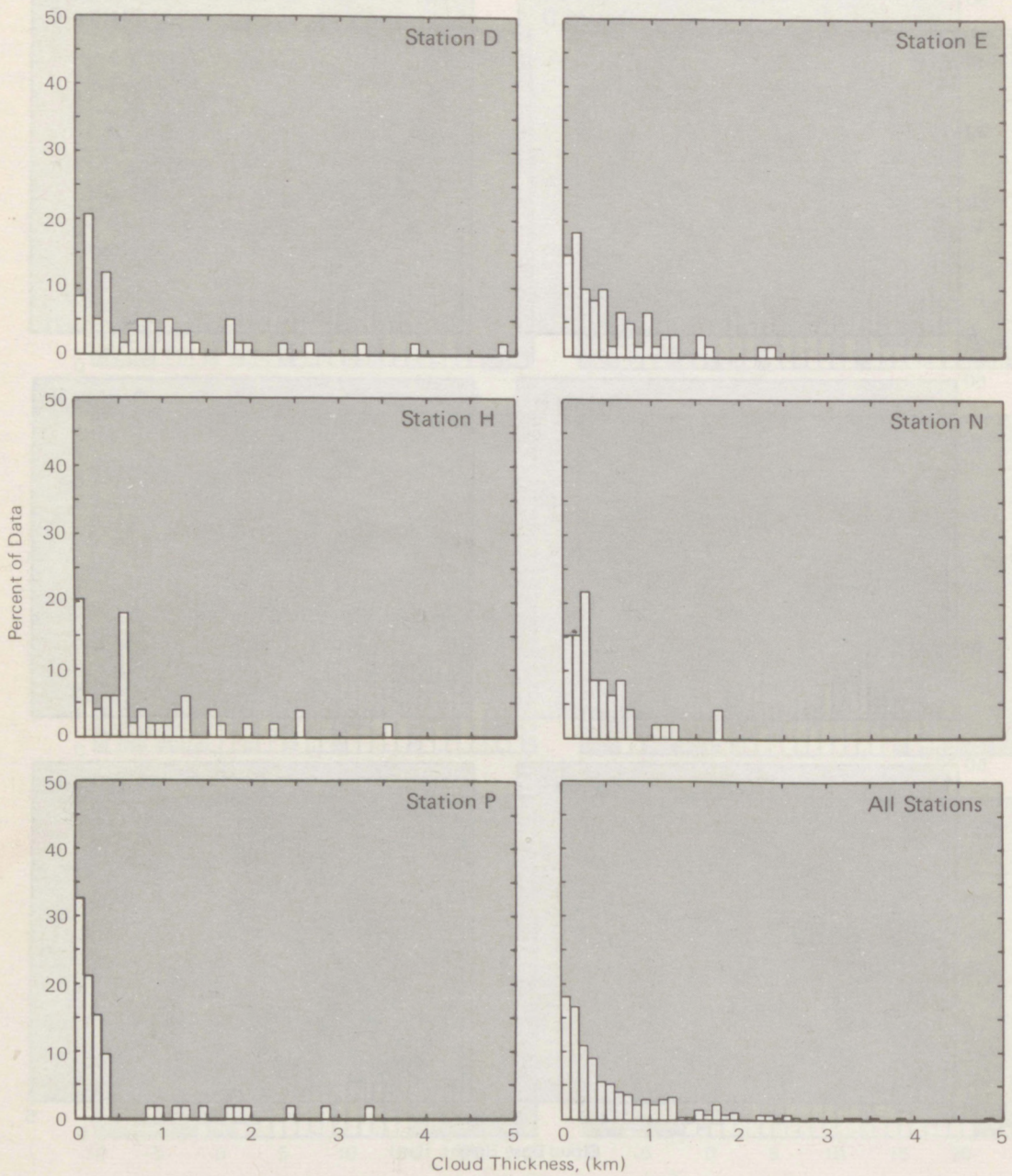

Figure 7. Histograms of cloud geometric thickness.

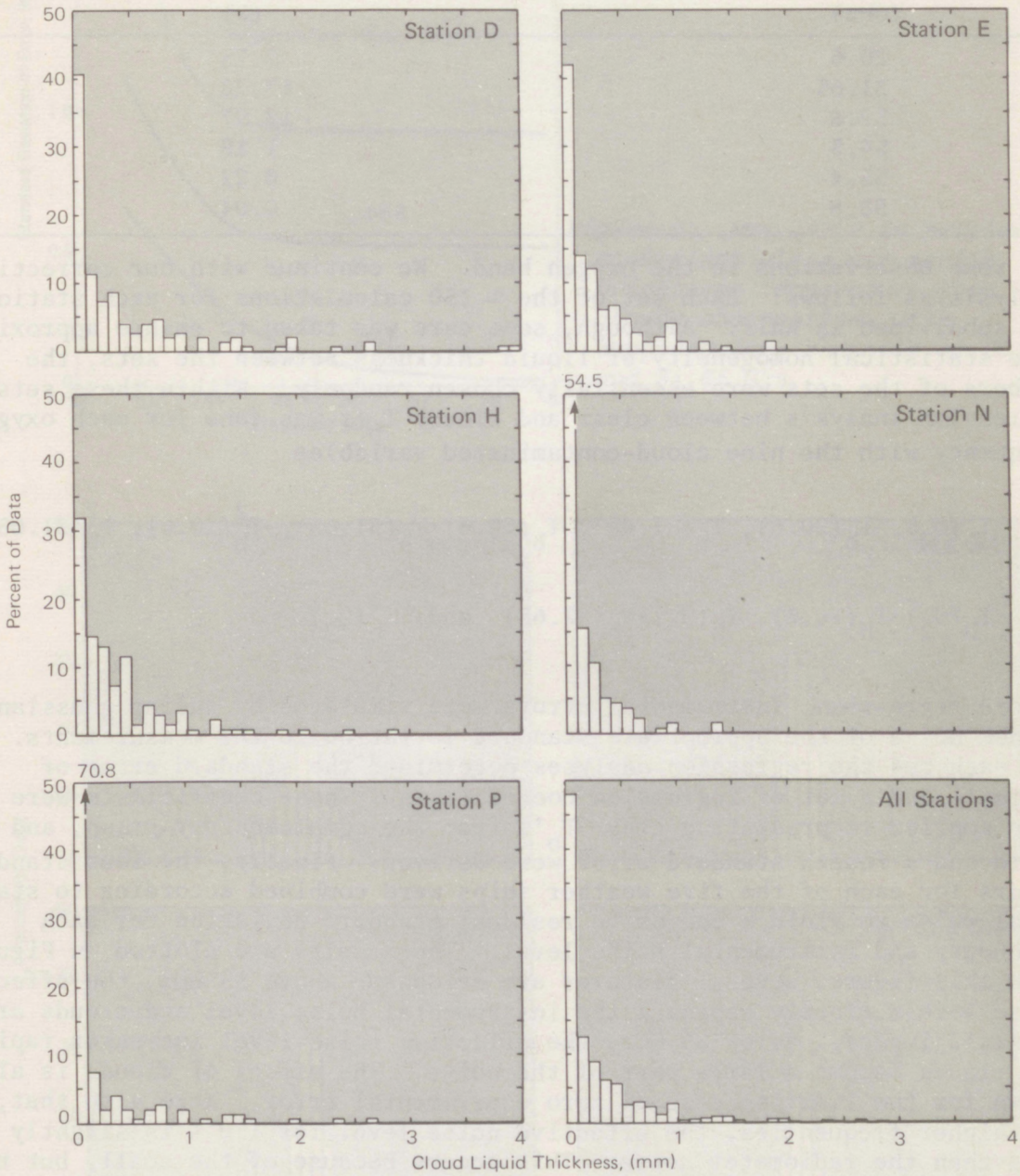

Figure 8. Histograms of cloud liquid thickness.

TABLE 2.

RMS Differences Between Clear and Cloudy
Zenith Brightness Temperatures (720 Profiles)

Frequency (GHz)	RMS Difference (K)
20.6	7.75
31.65	17.28
52.8	12.97
54.5	1.19
55.4	0.22
58.8	0.04

for some observations in the oxygen band. We continue with our correction analysis as follows: Each set of the $\sim$ 150 calculations for each station was subdivided in half. Although, some care was taken to ensure approximate statistical homogeneity of liquid thickness between the sets, the members of the sets were essentially chosen randomly. Within these sets, a regression analysis between clear and cloudy T_b's was done for each oxygen frequency with the nine cloud-contaminated variables

$$T_b(O_2),\ T_b(20.6),\ T_b(31.65),\ T_b(20.6)\cdot T_b(31.65),\ T_b^2(20.6),\ T_b^2(31.65),$$

$$T_b(O_2)\cdot T_b(20.6),\ T_b(O_2)\cdot T_b(31.65) \quad \text{and} \quad T_b^2(O_2).$$

Before regression, instrumental errors were simulated by adding gaussian random noise of the appropriate standard deviation to the measurements. For each set the regression analyses determined the standard error of estimate and a set of regression coefficients. These coefficients were in turn applied to predicting clear T_b's from the complementary group, and a third and a fourth standard error were derived. Finally, the four standard errors for each of the five weather ships were combined according to statistical rules to yield a composite residual standard deviation for each frequency and instrumental noise level. The results are plotted in Figure 9. From this figure, several features are evident: Above 55 GHz, the effective noise levels closely approach the instrumental noise level and clouds are of small impact. Below 55 GHz, the effective noise level increases rapidly and clouds become a large part of the noise. The effect of clouds is also shown for the limiting case of zero experimental error. Note also that, at the higher frequencies, the effective noise level for 1.0 K is slightly less than the radiometer noise. This occurs because of the small, but non-zero, correlation of the emissions at 20 and 31 GHz with temperature.

At each frequency the statistical distribution of errors was studied by histogram analysis. The distributions appeared to be gaussian, although no rigorous confidence tests were applied to this hypothesis. Figure 10 shows the histograms of all data for each frequency.

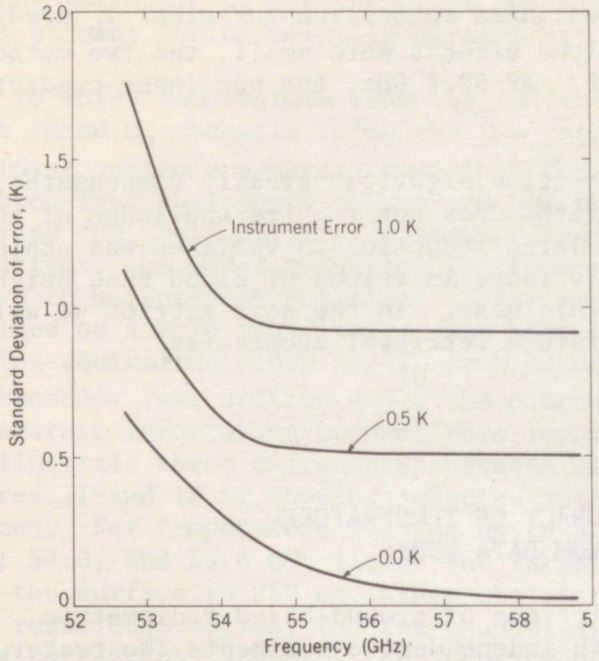

Figure 9. Rms error in retrieving equivalent clear air zenith brightness temperature from cloudy observations with supplementary channels at 20.6 and 31.65 GHz.

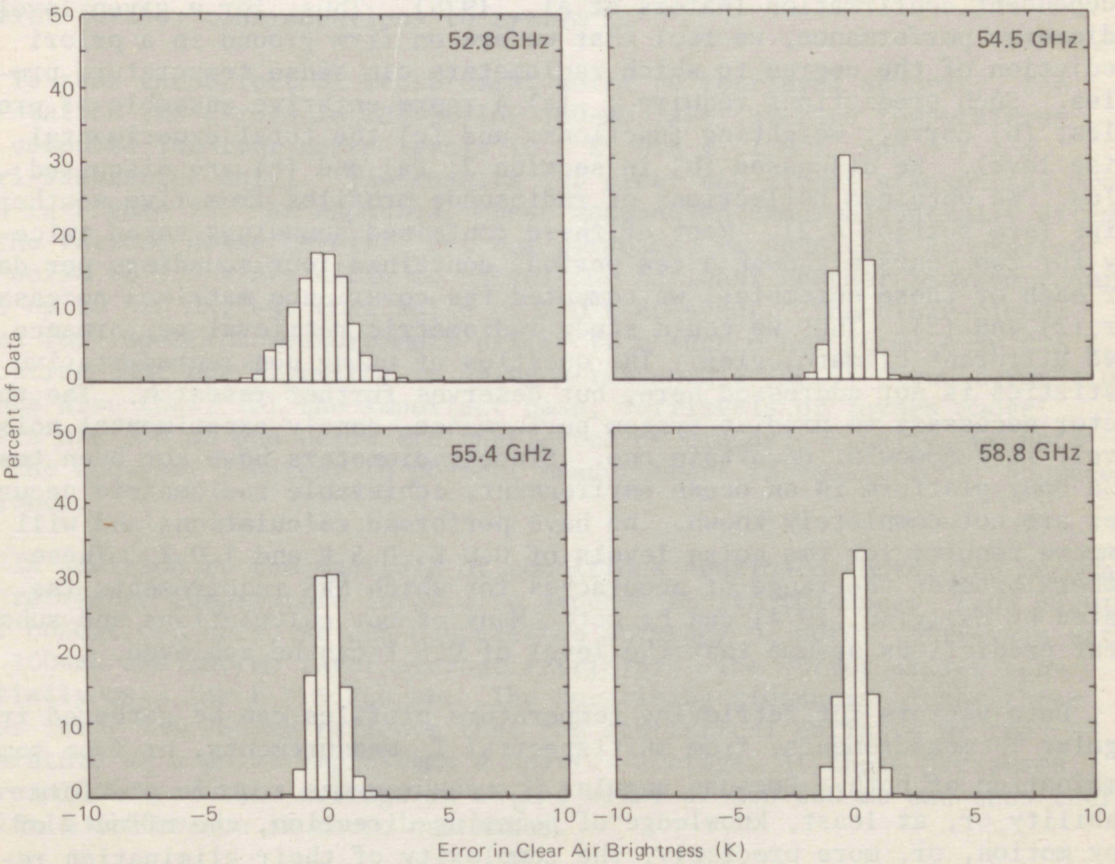

Figure 10. Histogram of errors in retrieving equivalent clear air zenith brightness temperature. Instrumental noise = 0.5 K.

We also compared linear and nonlinear regression for clear T_b prediction. At the frequencies for which the cloud effects were small, the two methods gave essentially the same rms error. At 52.8 GHz, the nonlinear predictors were superior by about 40%.

As shown above, our cloud correction algorithm greatly compensates for the presence of clouds. This algorithm does not require knowledge of the details of cloud structure and the large reduction in variance was achieved even though there was a considerable range in values of cloud base height, cloud base temperature, and cloud thickness. In the next section we will compare the clear and cloudy temperature retrieval accuracies.

5. PREDICTED ACCURACY OF TEMPERATURE RETRIEVALS FROM DATA BUOYS

In the past, statistical predictions of ground-based radiometric capabilities have compared well with independent experiments (Westwater, 1972; Snider, 1972; Westwater et al., 1975). Accuracy predictions of microwave temperature retrievals from a satellite have also achieved strong independent confirmation (Waters et al., 1975). Thus, for a given level of radiometer performance, we feel that we are on firm ground in a priori prediction of the degree to which radiometers can sense temperature profiles. Such predictions require : (a) a representative ensemble of profiles; (b) correct weighting functions; and (c) the total experimental noise level. We discussed (b) in section 2; (a) and (c) are discussed below. We obtained collections of radiosonde profiles from five weather ships (see section 4.2). Most of these contained soundings taken twice-a-day for two years although a few periods contained four soundings per day. For each of these ensembles, we computed the covariance matrices necessary for (2) and (3). Thus we could study radiometric retrieval performance for five different climatologies. The question of using non-representative statistics is not addressed here, but deserves further research. The third factor necessary to predict system performance, namely experimental noise level, is a somewhat uncertain one. Since radiometers have not been tested on a buoy platform in an ocean environment, achievable radiometric accuracies are not completely known. We have performed calculations and will compare results for rms noise levels of 0.0 K, 0.5 K and 1.0 K. These numbers bracket the range of accuracies for which NWS requirements (as stated by Hallgren, 1974) can be met. Many of our calculations and subsequent predictions assume that the level of 0.5 K can be achieved.

Data vectors for retrieving temperature profiles can be gathered from angular T_b measurements, from multispectral T_b measurements, or from some combination of both. Because angular T_b measurements require platform stability or, at least, knowledge of pointing direction, the effects of buoy motion, or, more precisely, the complexity of their elimination removed the angular scan from consideration (see the appendix for a discussion

of buoy motion). We are therefore considering only multi-frequency measurements at near zenith pointing directions.

To infer temperature from the surface to 500 mb, it was felt that at least three O_2 channels (plus the two water channels) were required. To determine suitable spectral positions for these channels, an extensive set of three-frequency combinations and one two-frequency combination were analyzed for their ability to recover temperature structure. During clear conditions, the total reduction in temperature variance was quite insensitive to measurement position. These results are consistent with those obtained on a more restrictive data base by Strand (1971). Because inferring equivalent clear air T_b from cloudy observations depends strongly on frequency (see section 4.3), the placement of frequencies to best obtain temperature information becomes more important during cloudy conditions. We illustrate these differences between clear and cloudy conditions in Figures 11 and 12 by showing selected sets of results for various frequency choices. For temperature sensing up to 500 mb, the system C choice of 52.8, 54.0, and 55.4 GHz yields the largest reduction in variance, although from the surface to 850 mb, other choices perform as well or better. For this restricted region, the two-channel system (which does not require cloud correction) achieves the accuracy of a five-channel system. Note also that the (optimum) retrievals during cloudy conditions are degraded by less than about 15 percent relative to clear. Because of these results, we restrict further considerations to system C.

To show the effect of measurement noise on retrieval accuracy, the five-station rms errors in retrieving 100-mb layer-average temperatures were computed for four noise levels (0.0 K, 0.5 K, 1.0 K, and ∞ K $\equiv$ a priori statistics only). The results for clear and cloudy atmospheres are shown in Figure 13. As expected, these accuracies are substantially different for the various noise levels. For our purposes, we note that accuracies with noise of 0.5 K are close to satisfying National Weather Service requirements up to 500 mb, but that noise of 1.0 K does not. The clear-cloudy curves for imperfect measurements differ from each other at most by 0.3 K, indicating that our algorithm is doing a reasonable job of cloud correction. We note also that, for the imperfect case, retrievals of layers whose centers are 850 mb and below are unaffected by clouds. Finally, we note that the accuracy inherent in perfect measurements is considerably degraded by clouds.

In addition to the manifold of conditions mentioned above, the accuracy of a retrieved temperature layer also depends on its thickness. From Figure 14, clear conditions only, we can compare the accuracy of point retrievals with both 100-mb and 200-mb layer average retrievals. The curves differ substantially only for $P > \sim 750$ mb. The surprising closeness of the three curves for $P < \sim 750$ mb reflects that the statistical estimate of the temperature at a point represents a spatial average. At these pressures, the resolution of this average is of the order of 100-200 mb and thus there is little difference in these estimates.

The results to this point have been primarily confined to the rms average of five stations. There were, however, considerable climatological

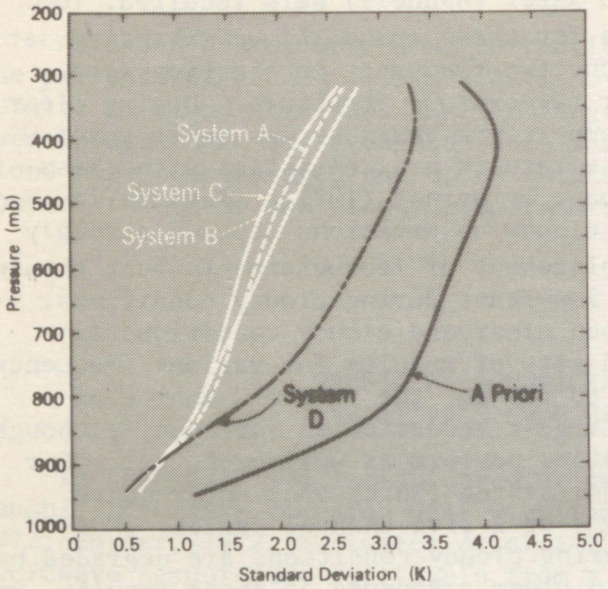

Figure 11. Comparison of several radiometric systems in retrieving temperature layers of 100-mb thickness during clear conditions. Five-station rms average. Instrumental error = 0.5 K.
Systems:
A(52.8, 55.4, 58.8, 20.6, 31.65 GHz);
B(54.0, 55.4, 58.8, 20.6, 31.65 GHz);
C(52.8, 54.0, 55.4, 20.6, 31.65 GHz);
D(55.4, 58.8 GHz).

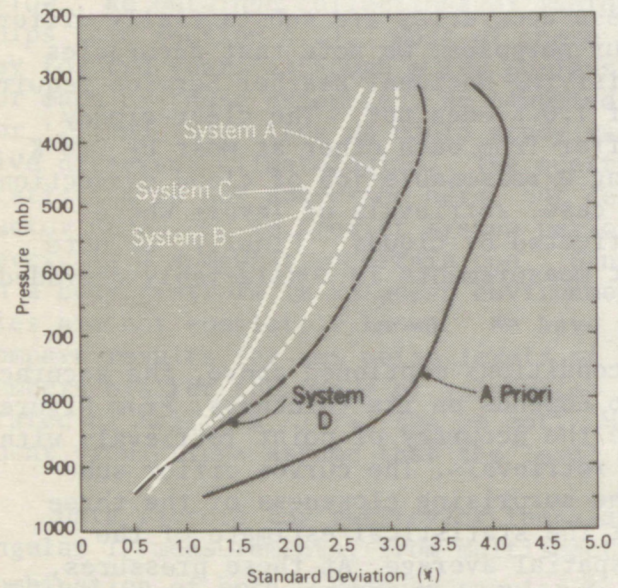

Figure 12. Comparison of several radiometric systems in retrieving temperature layers of 100-mb thickness during cloudy conditions (liquid thickness < 4 mm H_2O). Five-station rms average. Instrumental error = 0.5 K. Systems: same nomenclature as Figure 11.

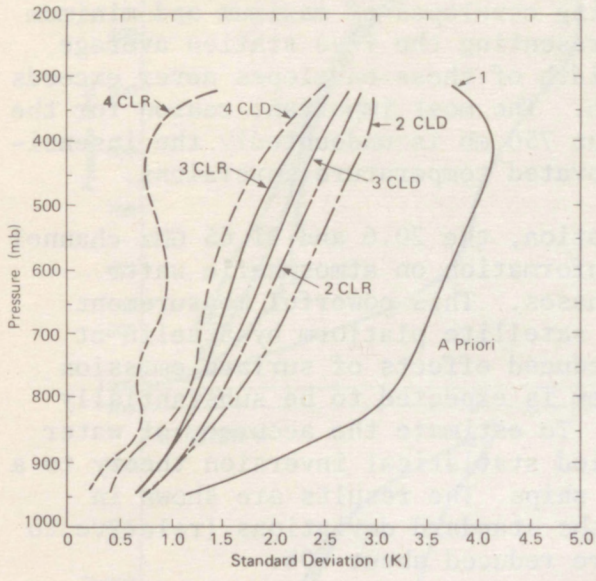

Figure 13. Comparison of clear (CLR) and cloudy (CLD) temperature retrievals for several instrumental noise levels. Layer thickness = 100-mb. Instrumental noise levels: 1 = ∞ K (a priori statistics), 2 = 1.0 K, 3 = 0.5 K, 4 = 0.0 K. Five stations. System C.

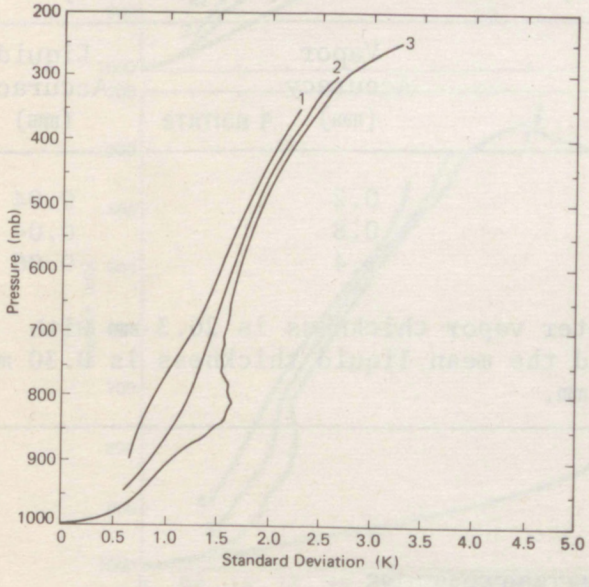

Figure 14. Comparison of rms accuracy in clear sky temperature retrievals for different layer thickness: 1 - 200 mb, 2 - 100 mb, 3 - point retrieval. Instrumental noise = 0.5 K. Five stations. System C.

variations between these stations, and, as a consequence, moderate variations in retrieval success. The rms accuracies in layer retrieval for each station are shown in Figures 15 and 16 for clear and cloudy conditions. For ease in comparison, the corresponding envelopes of maximum and minimum rms errors together with the curve representing the five station average are shown in Figures 17 and 18. The width of these envelopes never exceeds 0.8 K for pressures greater than 500 mb. The most important reason for the large variance at pressures greater than 750 mb is undoubtedly the insensitivity of the radiometric system to elevated temperature inversions.

In addition to temperature information, the 20.6 and 31.65 GHz channel system can also provide simultaneous information on atmospheric water content in both its liquid and vapor phases. This powerful measurement technique has been demonstrated from a satellite platform by Staelin et al., (1975). Because of the greatly reduced effects of surface emission the accuracy of a zenith-pointing system is expected to be substantially better than from a satellite platform. To estimate the accuracy of water thickness determination, we again applied statistical inversion theory to a composite ensemble of the five weather ships. The results are shown in Table 3. For a noise level of 0.5 K, the standard deviations (relative to their mean) of both liquid and vapor are reduced about 90%.

TABLE 3.

RMS Accuracy in the Retrieval of Water Thickness from Simulated Radiometric Observations at 20.6 and 31.65 GHz

RMS Instrument Error (K)	Clear Sky (240 Profiles)	Cloudy Sky (720 Profiles)	
	Vapor Accuracy (mm)	Vapor Accuracy (mm)	Liquid Accuracy (mm)
0.0	0.1	0.2	0.04
0.5	0.5	0.8	0.04
1.0	0.8	1.4	0.06

For these samples the mean water vapor thickness is 26.3 mm with a standard deviation of 10.5 mm and the mean liquid thickness is 0.30 mm with a standard deviation of 0.48 mm.

6. SUMMARY AND RECOMMENDATIONS

We have conducted a theoretical investigation into the feasibility of measuring atmospheric temperature structure by a microwave radiometer mounted on an ocean-based data buoy. Initially, both multi-spectral and angular scan measurements were considered. However, because of buoy motion,

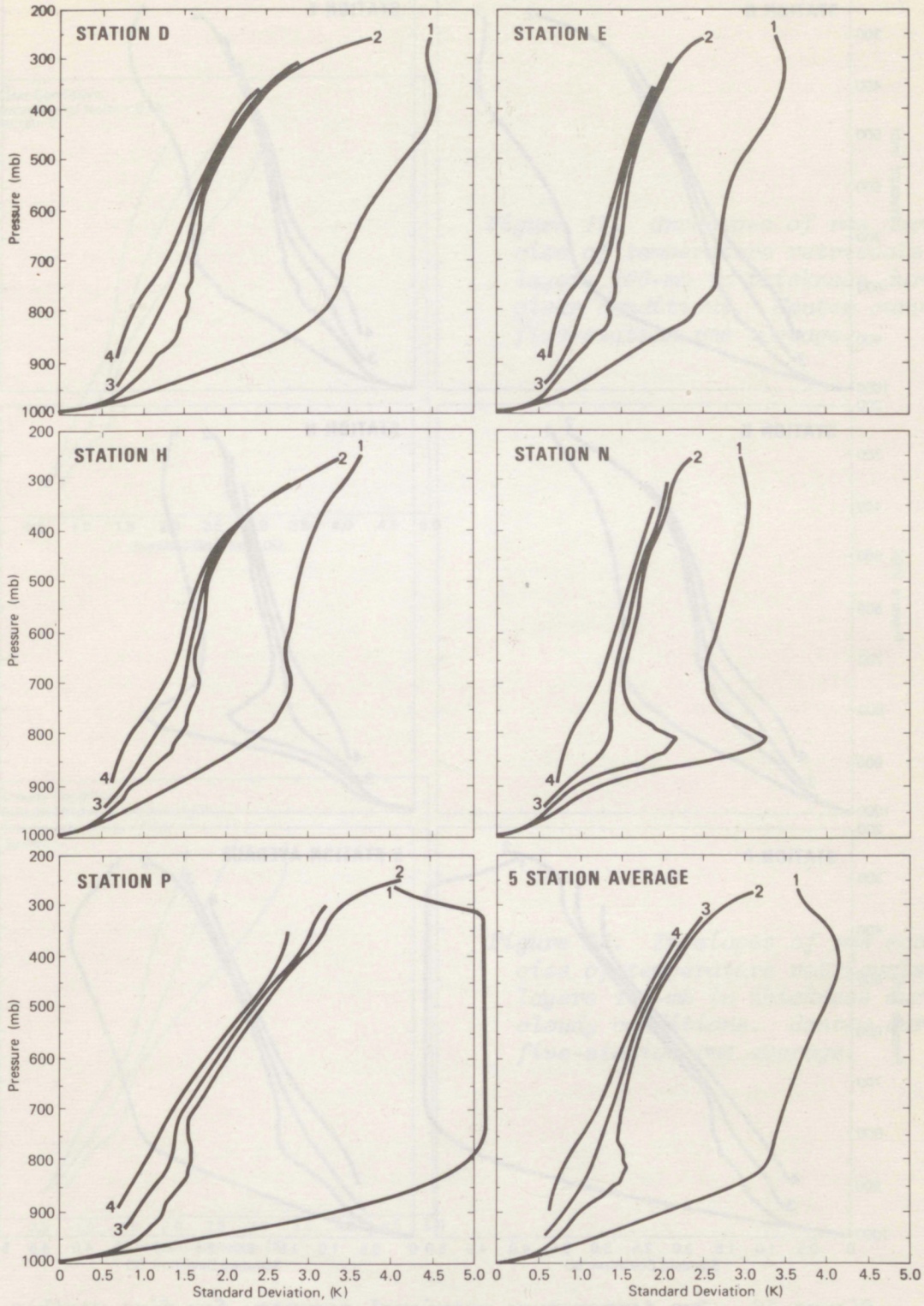

Figure 15. Rms temperature retrieval accuracy for five weather ships. Instrumental noise = 0.5 K. Clear conditions. 1 = a priori statistics only, 2 = point retrieval, 3 = 100-mb layer retrieval, 4 = 200-mb layer retrieval. System C.

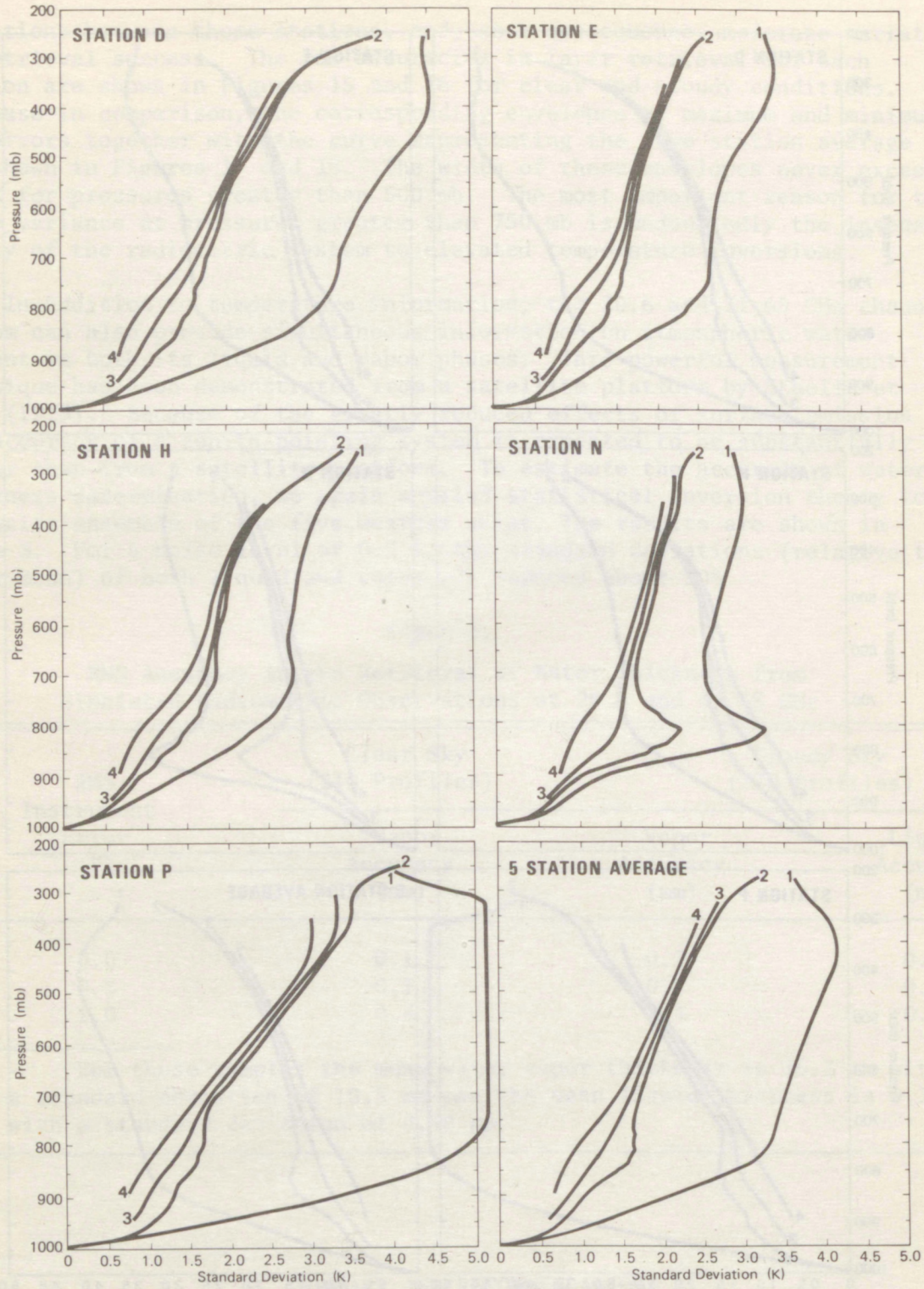

Figure 16. Rms temperature retrieval accuracy for five weather ships. Instrumental noise = 0.5 K. Cloudy conditions with liquid thickness < 4 mm H_2O. 1 = a priori statistics only, 2 = point retrieval, 3 = 100-mb layer retrieval, 4 = 200-mb layer retrieval. System C.

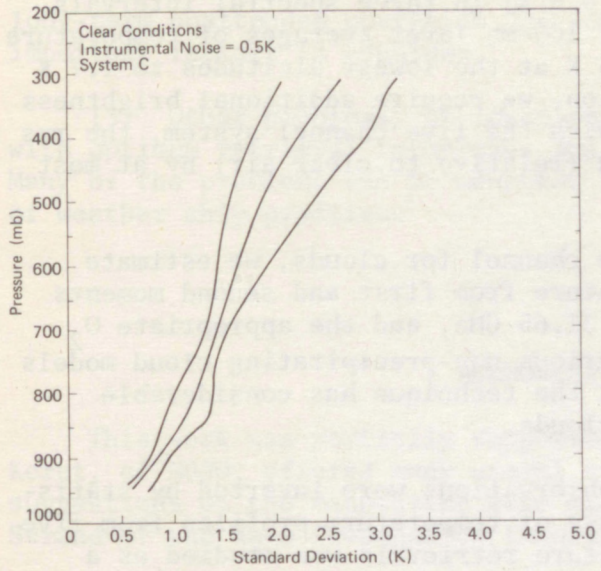

Figure 17. Envelopes of rms accuracies of temperature retrievals of layers 100-mb in thickness during clear conditions. Center curve is five-station rms average.

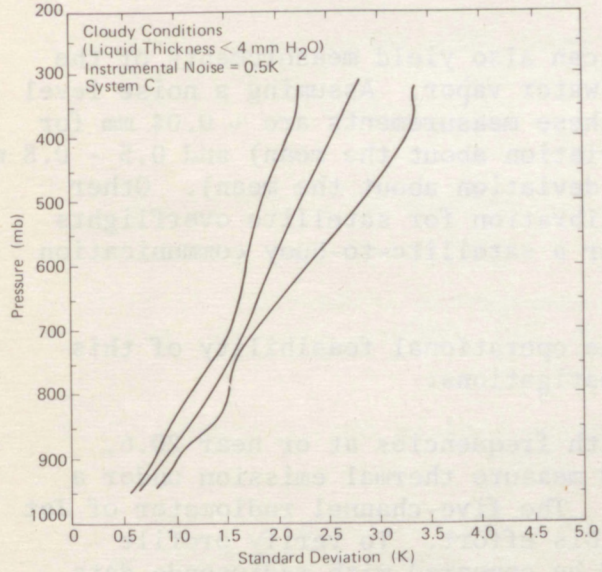

Figure 18. Envelopes of rms accuracies of temperature retrievals of layers 100-mb in thickness during cloudy conditions. Center curve is five-station rms average.

angular scan methods of brightness measurement were eliminated from consideration. During clear conditions, accurate zenith measurements of O_2 thermal emission (instrumental noise = 0.5 K) in three spectral intervals can be mathematically inverted to infer 100-mb layer averages of temperature with rms accuracies that range from 0.5 K at the lowest altitudes to 1.7 K at 500 mb. To correct for cloud emission, we require additional brightness measurements at $\sim$ 21 GHz and 31 GHz. With the five channel system, the rms temperature retrieval error is degraded (relative to clear air) by at most 0.3 K.

To correct a temperature sensitive channel for clouds, we estimate equivalent clear-air brightness temperature from first and second moments of cloudy T_b observations at 20.6 GHz, 31.65 GHz, and the appropriate O_2 channel. Computer simulations using various non-precipitating cloud models (liquid thickness < 4 mm) indicate that the technique has considerable potential for reducing the effects of clouds.

Simulated brightness temperature observations were inverted by statistical retrieval methods using a data base of temperature profiles from five weather ships. The accuracy of temperature retrievals was studied as a function of the following parameters: radiometer noise level, various choices of frequency, two vs. three channels, layer pressure thickness, clear vs. cloudy skies, and each of the five climatologies. On the basis of these simulations, we recommend that suitable locations for temperature channels are 52.8 GHz, 54.0 GHz, and 55.4 GHz. These simulations suggest that radiometer noise levels of 0.5 K or less must be achieved to provide temperature profile accuracies that are close to meeting requirements stated by the National Weather Service.

The two cloud correcting channels can also yield measurements of the integrated amounts of liquid water and water vapor. Assuming a noise level of 0.5 K, the estimated accuracies of these measurements are $\sim$ 0.04 mm for liquid ($\sim$ 90% reduction in standard deviation about the mean) and 0.5 - 0.8 mm for vapor ($\sim$ 95% reduction in standard deviation about the mean). Other possible uses of these channels are calibration for satellite overflights and microwave attenuation statistics for a satellite-to-buoy communication link.

As the next step in determining the operational feasibility of this system, we recommend the following investigations:

(1) A five-channel radiometer, with frequencies at or near 20.6, 31.65, 52.8, 54.0, and 55.4 GHz, should measure thermal emission under a variety of clear and cloudy conditions. The five-channel radiometer of Jet Propulsion Laboratory seems ideal for this effort. To verify profile retrieval algorithms, these data should be compared with radiosonde data taken nearly coincident in time and space. Initially, a ground-based experiment will suffice. If predicted accuracies are obtained a ship-based or a buoy-based experiment is the next logical step.

(2) An engineering design and cost analysis study should be undertaken to design a radiometer system to operate in an ocean environment. Environmental effects on the entire radiometer system, including antennas, long-term unattended operation and low power consumption are among the important factors to consider.

(3) Other problems, of lower priority than (1) and (2), are concerned with optimum retrieval techniques and updating of inversion coefficients. Many of the problems can be computer simulated with our existing data base of weather ship profiles.

ACKNOWLEDGMENTS

This work was partially supported by the NOAA Data Buoy Office. E. G. Kerut, of NDBO, offered many useful suggestions and guidelines. Valuable suggestions on the manuscript were made by J. B. Snider and Dr. O. N. Strand of the Wave Propagation Laboratory, NOAA.

REFERENCES

Carter, C. J., R. L. Mitchell, and E. E. Reber, Oxygen absorption measurements in the lower atmosphere. J. Geophy. Res. 72, 6137-6148, 1968.

Deutsch, R., Estimation Theory, Prentice-Hall, Inc., Englewood Cliffs, N.J., 269 pp. 1965.

Fowler, M. G., N. D. Sze, N. E. Gaut, The estimation of clear sky emission values from cloudy radiometric data. Air Force Cambridge Research Laboratories - TR-75-0440. 57 pp, 1975.

Hallgren, R. E., Private Communication, 1974.

Hosler, C. R. and T. J. Lemmons, Radiometric measurements of temperature profiles in the planetary boundary layer. J. Appl. Meteor. 11, 341-348, 1972.

Laws, J. O. and Parsons, D. A., The relation of raindrop size to intensity Trans. Amer. Geophys. Union. 24, 432-460, 1943.

Liebe, H. J., Calculated tropospheric dispersion and absorption due to the 22-GHz water vapor line. IEEE Trans. Ant. Prop. AP-17, 621-627, 1969.

Liebe, H. J., Molecular transfer characteristics of air between 40 and 140 GHz. IEEE Trans. Microwave Theory Tech. MTT-23, 380-386, 1975.

Miner, G. F., D. D. Thornton and W. J. Welch, The inference of atmospheric temperature profiles from ground-based measurements of microwave emission from atmospheric oxygen. J. Geophys. Res. 77, 975-991, 1972.

Platt, C. M. R., Lidar and radiometric observations of cirrus clouds. J. Atmos. Sci. 30, 1191-1204, 1973.

Rodgers, C. D., Remote sounding of the atmospheric temperature profile in the presence of cloud. Quart. J. Roy. Meteor. Soc., 96, 654-666, 1970.

Rosenkranz, P. W., Shape of the 5-mm oxygen band in the atmosphere. IEEE Trans. Ant. Prop., AP-23, 498-506, 1975.

Smith, W. L., H. M. Woolf and W. J. Jacob, A regression method for obtaining real-time temperature and geopotential height profiles from satellite spectrometer measurements and its application to Nimbus 3 SIRS observations. Mon. Wea. Rev., 98, 582-603, 1970.

Snider, J. B., Ground-based sensing of temperature profiles from angular and multi-spectral microwave emission measurements. J. Appl. Meteor., 11, 958-967, 1972.

Snider, J. B. and E. R. Westwater, Atmospheric attenuation at 15, 31, and 53 GHz. ESSA Tech. Rept. ERL 156-WPL 11, 84 pp, 1969.

Staelin, D. H., A. L. Cassel, K. F. Kunzi, R. L. Pettyjohn, R. K. L. Poon, P. W. Rosenkranz, and J. W. Waters, Microwave atmospheric temperature sounding: effects of clouds on the Nimbus 5 satellite data. J. Atmos. Sci., 32, 1970-1976, 1975.

Strand, O. N., Optimization of frequencies used in indirect sensing by inversion. NOAA Tech. Rept. ERL 202-WPL 14. 22 pp, 1975.

Waters, J. W., K. F. Kunzi, R. L. Pettyjohn, R. K. L. Poon and D. H. Staelin, Remote sensing of atmospheric temperature profiles with the Nimbus 5 microwave spectrometer. J. Atmos. Sci., 32, 1953-1969, 1975.

Westwater, E. R., Ground-based determination of low-altitude temperatures by microwaves. Mon. Wea. Rev. 100, 15-28, 1972.

Westwater, E. R., J. B. Snider and A. V. Carlson, Experimental determination of temperature profiles by ground-based microwave radiometry. J. Appl. Meteor. 14, 524-539, 1975.

Van Vleck, J. H., The absorption of microwaves by oxygen. Phys. Rev. 71, 413-424, 1947a.

Van Vleck, J. H., The absorption of microwaves by uncondensed water vapor. Phys. Rev. 71, 425-433, 1947b.

APPENDIX. EFFECTS OF BUOY MOTION ON OBSERVED MICROWAVE BRIGHTNESS TEMPERATURE

The brightness temperature of the sky varies with the zenith angle. Examples of this variation (Figure A-1) clearly show that pitch angle motion of the data buoy must be considered in the design of a radiometric system. Note that near zenith, the brightness temperature changes rather slowly with zenith angle, and that for a clear sky the minimum T_b will be at the zenith.

To evaluate the magnitude of change in T_b with expected pitch angles we simulated the motion of the NDBO Prototype Environmental Buoy (PEB) with sea-state conditions expected in the Gulf of Alaska. Data supplied by NDBO give the response of the buoy in terms of the pitch angle spectrum for a large range of combinations of significant wave height and mean wave period. From these data the standard deviation of the pitch angle may be found, and in Figure A-2 we have plotted contours of pitch angle standard deviation as a function of sea state parameters. It can be seen that the same pitch angle amplitude spectrum can result from various combinations of these variables, although the pitch rate spectrum would be quite different. Additional data supplied by NDBO show the frequency of occurrence of all

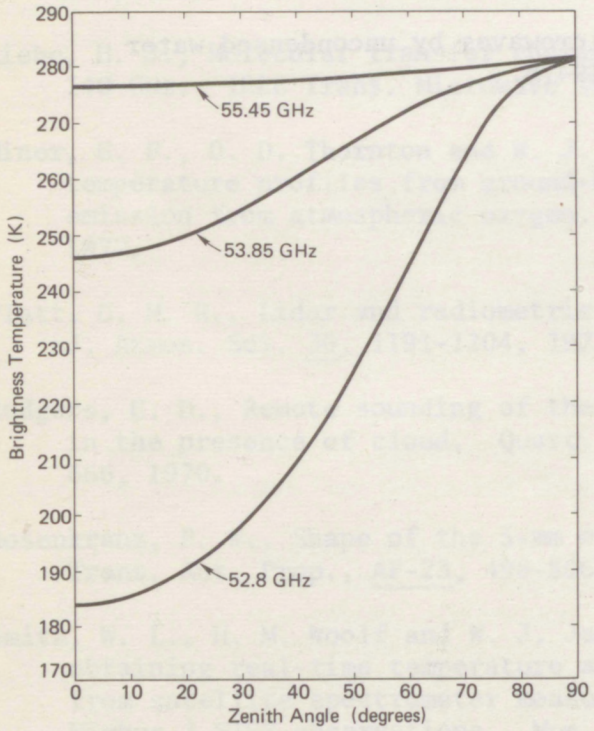

Figure A-1. Brightness temperature of the mean clear atmosphere at Ocean Station P for the three oxygen channels of System C of the main report.

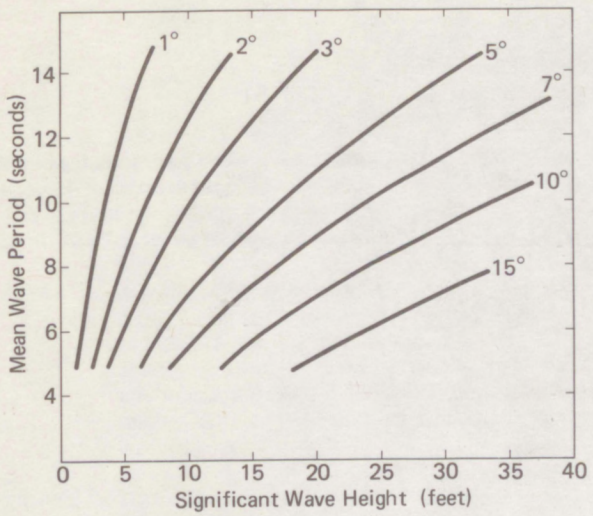

Figure A-2. Contours of the standard deviation of the PEB buoy pitch-angle distribution for the indicated combination of wave height and period.

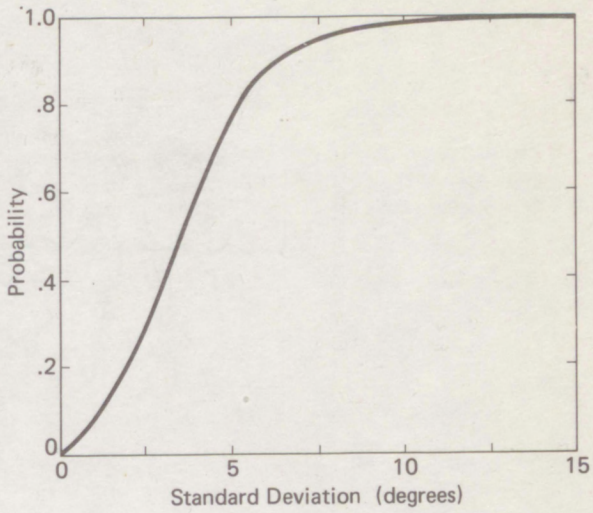

Figure A-3. Probability that the standard deviation of the PEB buoy pitch-angle distribution is less than the indicated value for sea-state conditions in the Gulf of Alaska.

combinations of significant wave height and period as observed at Ocean Station "P" in the Gulf of Alaska, so that we may derive the cumulative probability that the standard deviation of the pitch angle is less than a given value. This curve is shown in Figure A-3, which shows, for example, that for 78% of the time the standard deviation of the pitch angle would be less than 5°, and for 98% of the time it would be less than 10°. Brief time series of pitch angle with these two standard deviations were generated and are shown in Figures A-4 and A-5, along with examples of brightness temperatures in the direction of the vertical axis of the buoy. These brightness temperatures might be observed at a frequency of 52.8 GHz, while at higher frequencies in the oxygen complex the variation in brightness temperature would be less. It is assumed in these calculations that the buoy oscillates in a vertical plane, and hence the minimum brightness temperature is the zenith value. If appropriate radiometer time constants are incorporated, the information contained in the brightness temperature vs. time record could be used to greatly reduce the fluctuations that are observed. For a radiometer pointing at other elevation angles, the variation in observed brightness temperatures would generally be much greater, and it would be more difficult to determine the appropriate brightness temperature. For this reason we have restricted ourselves in the main body of this paper to a multi-frequency zenith-pointing system.

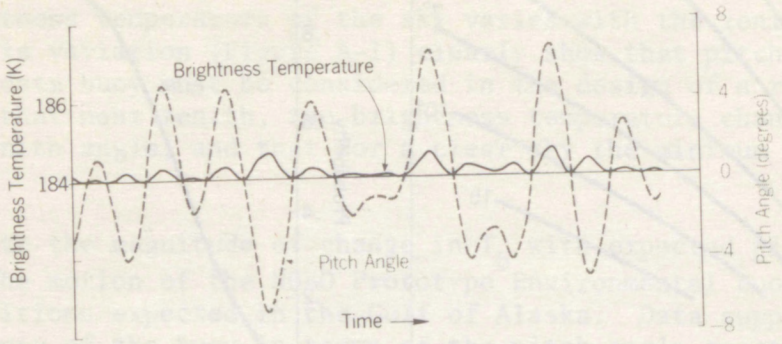

Figure A-4. Buoy pitch-angle variation and resulting change in observed brightness temperature at 52.8 GHz for a pitch-angle standard deviation of 5°.

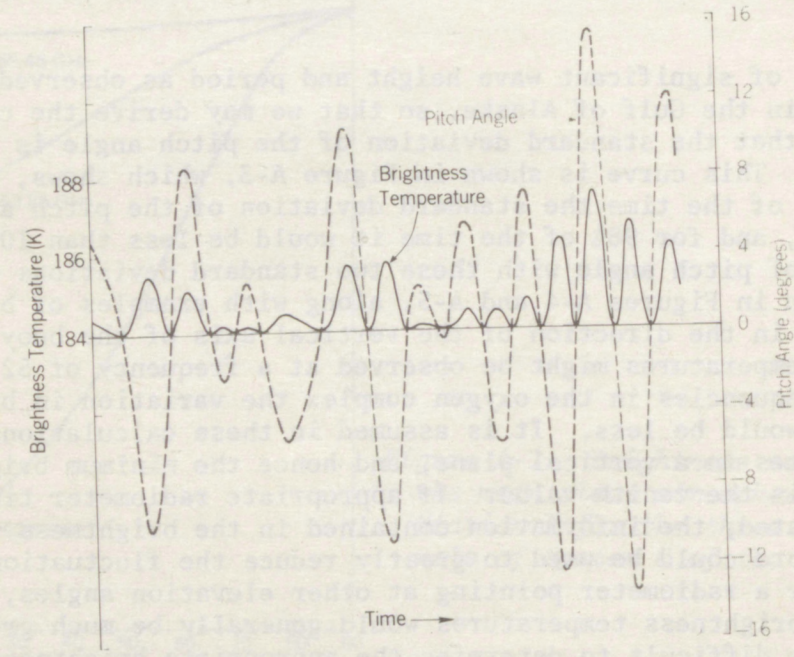

Figure A-5. Buoy pitch-angle variation and resulting change in observed brightness temperature at 52.8 GHz for a pitch-angle standard deviation of 10°.

☆ U. S. GOVERNMENT PRINTING OFFICE: 1976—677-347/1289 REGION NO. 8

Environmental Research LABORATORIES

The mission of the Environmental Research Laboratories (ERL) is to conduct an integrated program of fundamental research, related technology development, and services to improve understanding and prediction of the geophysical environment comprising the oceans and inland waters, the lower and upper atmosphere, the space environment, and the Earth. The following participate in the ERL missions:

MESA *Marine EcoSystems Analysis Program.* Plans, directs, and coordinates the regional projects of NOAA and other federal agencies to assess the effect of ocean dumping, municipal and industrial waste discharge, deep ocean mining, and similar activities on marine ecosystems.

OCSEA *Outer Continental Shelf Environmental Assessment Program.* Plans, directs, and coordinates research of federal, state, and private institutions to assess the primary environmental impact of developing petroleum and other energy resources along the outer continental shelf of the United States.

WM *Weather Modification Program Office.* Plans, directs, and coordinates research within ERL relating to precipitation enhancement and mitigation of severe storms. Its National Hurricane and Experimental Meteorology Laboratory (NHEML) studies hurricane and tropical cumulus systems to experiment with methods for their beneficial modification and to develop techniques for better forecasting of tropical weather. The Research Facilities Center (RFC) maintains and operates aircraft and aircraft instrumentation for research programs of ERL and other government agencies.

AOML *Atlantic Oceanographic and Meteorological Laboratories.* Studies the physical, chemical, and geological characteristics and processes of the ocean waters, the sea floor, and the atmosphere above the ocean.

PMEL *Pacific Marine Environmental Laboratory.* Monitors and predicts the physical and biological effects of man's activities on Pacific Coast estuarine, coastal, deep-ocean, and near-shore marine environments.

GLERL *Great Lakes Environmental Research Laboratory.* Studies hydrology, waves, currents, lake levels, biological and chemical processes, and lake-air interaction in the Great Lakes and their watersheds; forecasts lake ice conditions.

GFDL *Geophysical Fluid Dynamics Laboratory.* Studies the dynamics of geophysical fluid systems (the atmosphere, the hydrosphere, and the cryosphere) through theoretical analysis and numerical simulation using powerful, high-speed digital computers.

APCL *Atmospheric Physics and Chemistry Laboratory.* Studies cloud and precipitation physics, chemical and particulate composition of the atmosphere, atmospheric electricity, and atmospheric heat transfer, with focus on developing methods of beneficial weather modification.

NSSL *National Severe Storms Laboratory.* Studies severe-storm circulation and dynamics, and develops techniques to detect and predict tornadoes, thunderstorms, and squall lines.

WPL *Wave Propagation Laboratory.* Studies the propagation of sound waves and electromagnetic waves at millimeter, infrared, and optical frequencies to develop new methods for remote measuring of the geophysical environment.

ARL *Air Resources Laboratories.* Studies the diffusion, transport, and dissipation of atmospheric pollutants; develops methods of predicting and controlling atmospheric pollution; monitors the global physical environment to detect climatic change.

AL *Aeronomy Laboratory.* Studies the physical and chemical processes of the stratosphere, ionosphere, and exosphere of the Earth and other planets, and their effect on high-altitude meteorological phenomena.

SEL *Space Environment Laboratory.* Studies solar-terrestrial physics (interplanetary, magnetospheric, and ionospheric); develops techniques for forecasting solar disturbances; provides real-time monitoring and forecasting of the space environment.

U.S. DEPARTMENT OF COMMERCE
National Oceanic and Atmospheric Administration
BOULDER, COLORADO 80302